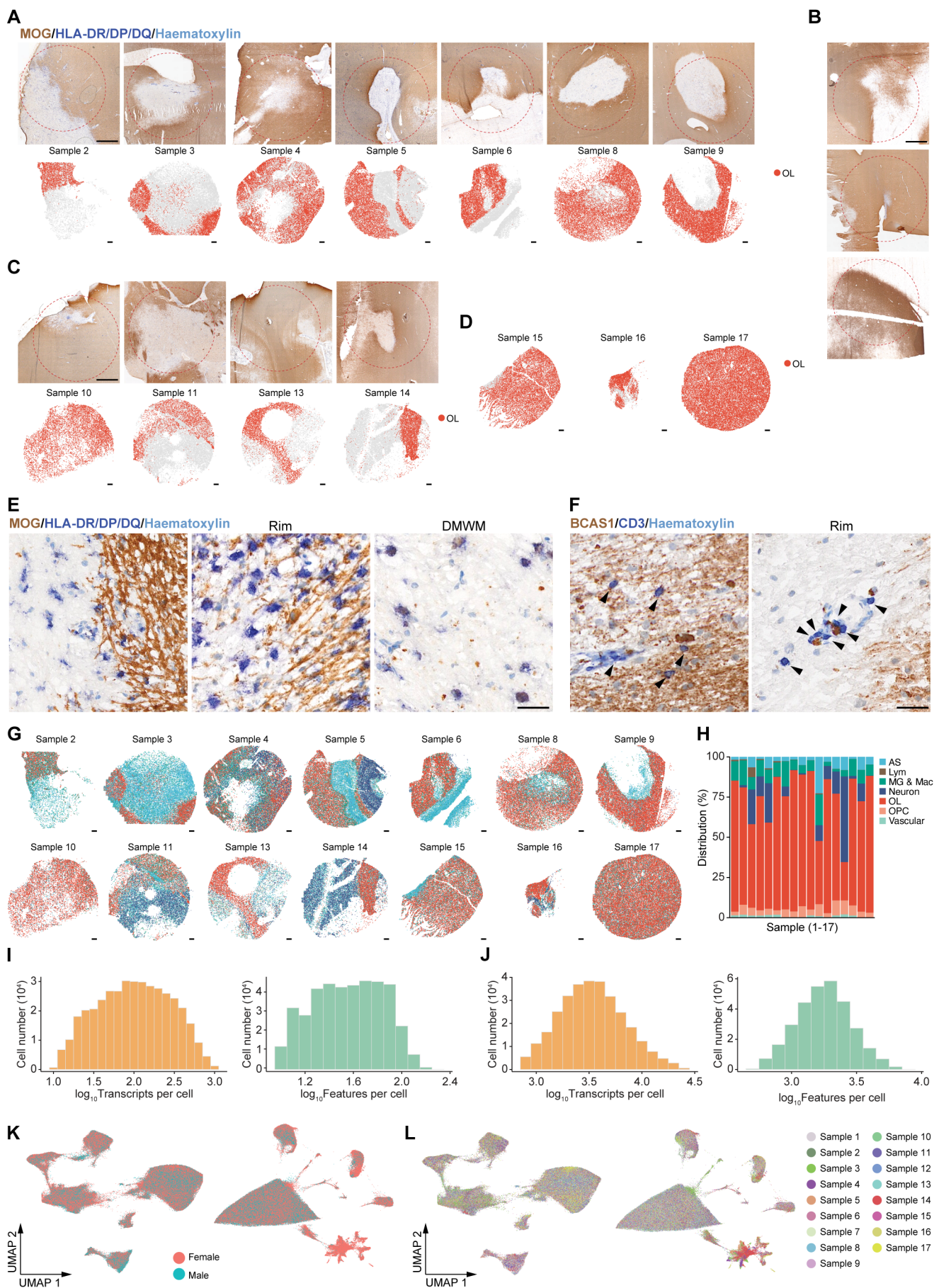


Supplemental information

**Single-cell spatial transcriptomic profiling
defines a pathogenic inflammatory niche
in chronic active multiple sclerosis lesions**

Ruoqing Feng, Lena Spieth, Lu Liu, Stefan Berghoff, Jonas Franz, Qian Liu, Zhen Wang, Vini Tiwari, Simona Vitale, Simon Frerich, Sergi Florensa, Niklas Junker, Ludwig Huber, Marco Keller, Christoph Müller, Franz Bracher, Xiaoke Ge, Patrick C.N. Rensen, Gijs Kooij, Leon Hosang, Serhii Chorny, Martin Dichgans, Ozgun Gokce, Gesine Saher, Christine Stadelmann, Martin Giera, Janos Groh, and Mikael Simons



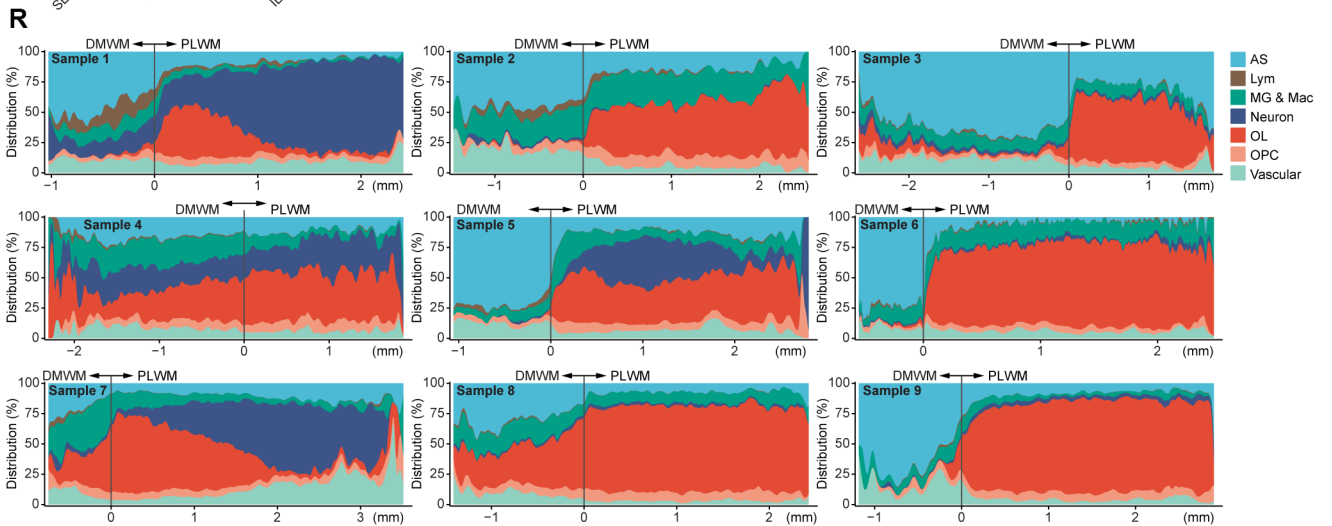
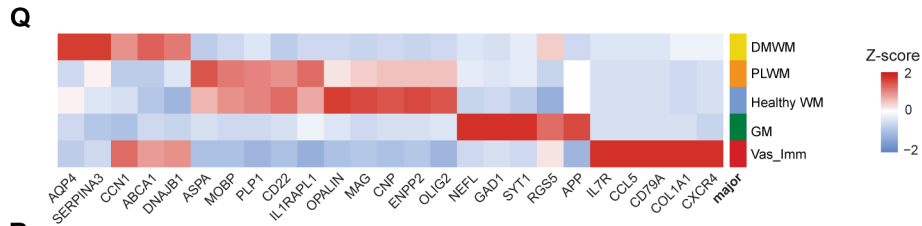
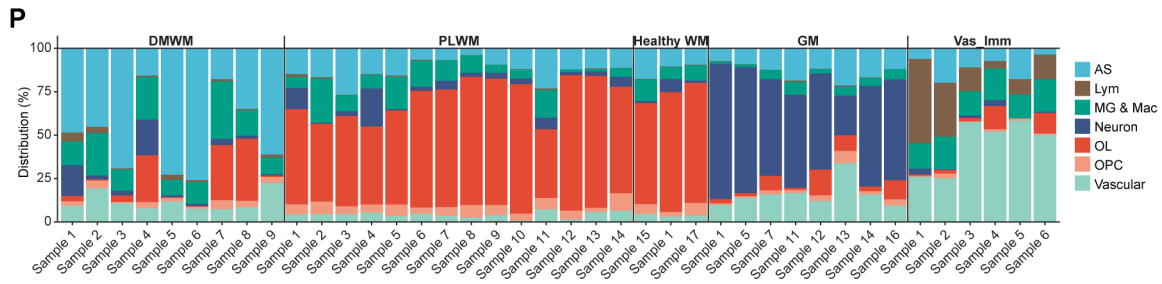
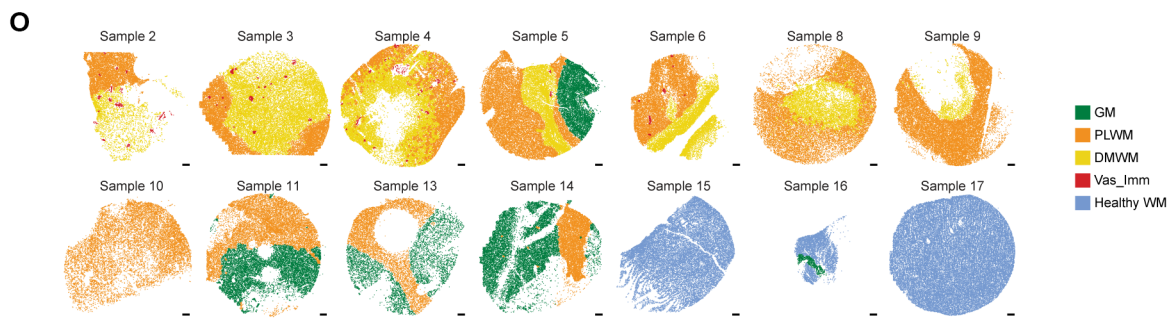
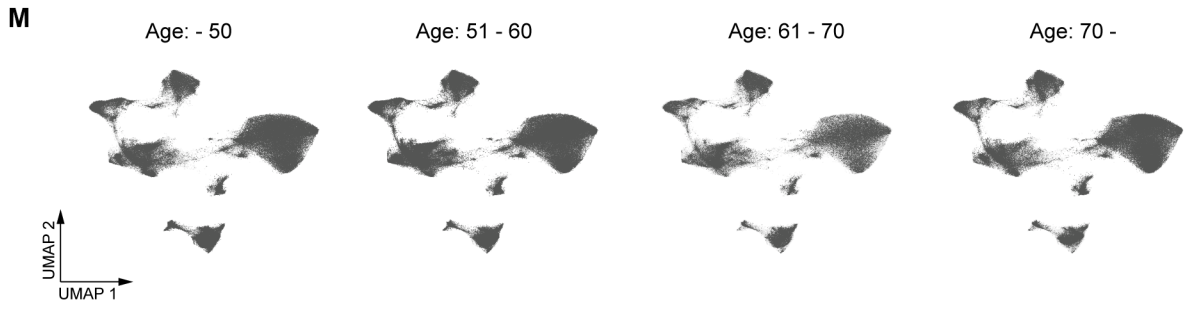


Figure S1. Histopathological and single-cell spatial transcriptomic characterization reveals hallmarks of human MS lesions, Related to Figure 1

(A and C) Immunohistochemical detection of MOG, HLA-DR/DP/DQ (top), and spatial mapping of oligodendrocytes (bottom) identified by MERFISH and projected onto matching adjacent sections from the same individuals with MS. Sections with (panel A) or without (panel C) captured DMWM in addition to PLWM are shown. Scale bars, top: 2 mm, bottom: 400 μ m.

(B) Immunohistochemical detection of MOG and HLA-DR/DP/DQ in adjacent sections from 3 individuals with MS as shown in Figure 1D. Scale bar, 2 mm. Red dashed circles indicate target region for punch sampling. Nuclei are labelled with haematoxylin.

(D) Spatial mapping of oligodendrocytes (bottom) identified by MERFISH and projected onto sections from 3 healthy individuals. Scale bar, 400 μ m.

(E) Immunohistochemical detection of MOG and HLA-DR/DP/DQ in sections from individuals with MS at the lesion rim or in the lesion core (DMWM). Scale bar, 50 μ m.

(F) Immunohistochemical detection of BCAS1 and CD3 in sections from individuals with MS at the lesion rim. Arrowheads indicate T cells in the parenchyma and perivascular regions. Scale bar, 50 μ m.

(G) Spatial mapping of all major cell types identified by MERFISH and projected onto 11 sections from different MS patients and 3 sections from healthy individuals. Scale bars, 400 μ m.

(H) Bar plot showing the distribution of major cell types across all samples (snRNA-seq dataset).

(I) Histogram showing the transcript counts (left) and feature counts (right) of all cells identified by MERFISH.

(J) Histogram showing the transcript counts (left) and feature counts (right) of all nuclei identified by snRNA-seq.

(K) Projection of donor sex onto the UMAP for the MERFISH (left) and snRNA-seq (right) datasets.

(L) Projection of sample information onto the UMAP for the MERFISH (left) and snRNA-seq (right) datasets.

(M) Samples were divided according to donor age into four groups (≤ 50 years, 51-60 years, 61-70 years, and ≥ 71 years) and projected onto the UMAP for the MERFISH and (N) snRNA-seq datasets.

(O) Spatial mapping of cells identified by MERFISH and projected onto 11 sections from different MS patients and 3 sections from healthy individuals after BANKSY domain segmentation. Scale bars, 400 μ m.

(P) Bar plot showing the distribution of major cell types across each sample as identified by MERFISH in all BANKSY-segmented domains (DMWM, PLWM, healthy WM, GM, and Imm_vas).

(Q) Heatmap of scaled average expression for selected marker genes of all cells across different BANKSY domains in the MERFISH dataset.

(R) Density plots illustrate the distribution of major cell types along the SPATA2 spatial gradient, according to the annotation of the DMWM and PLWM; the lesion boundary and inwards/outwards distances are indicated.

DMWM, demyelinated white matter; PLWM, perilesional white matter; GM, grey matter; Vas_Imm, perivascular immune cell domain.

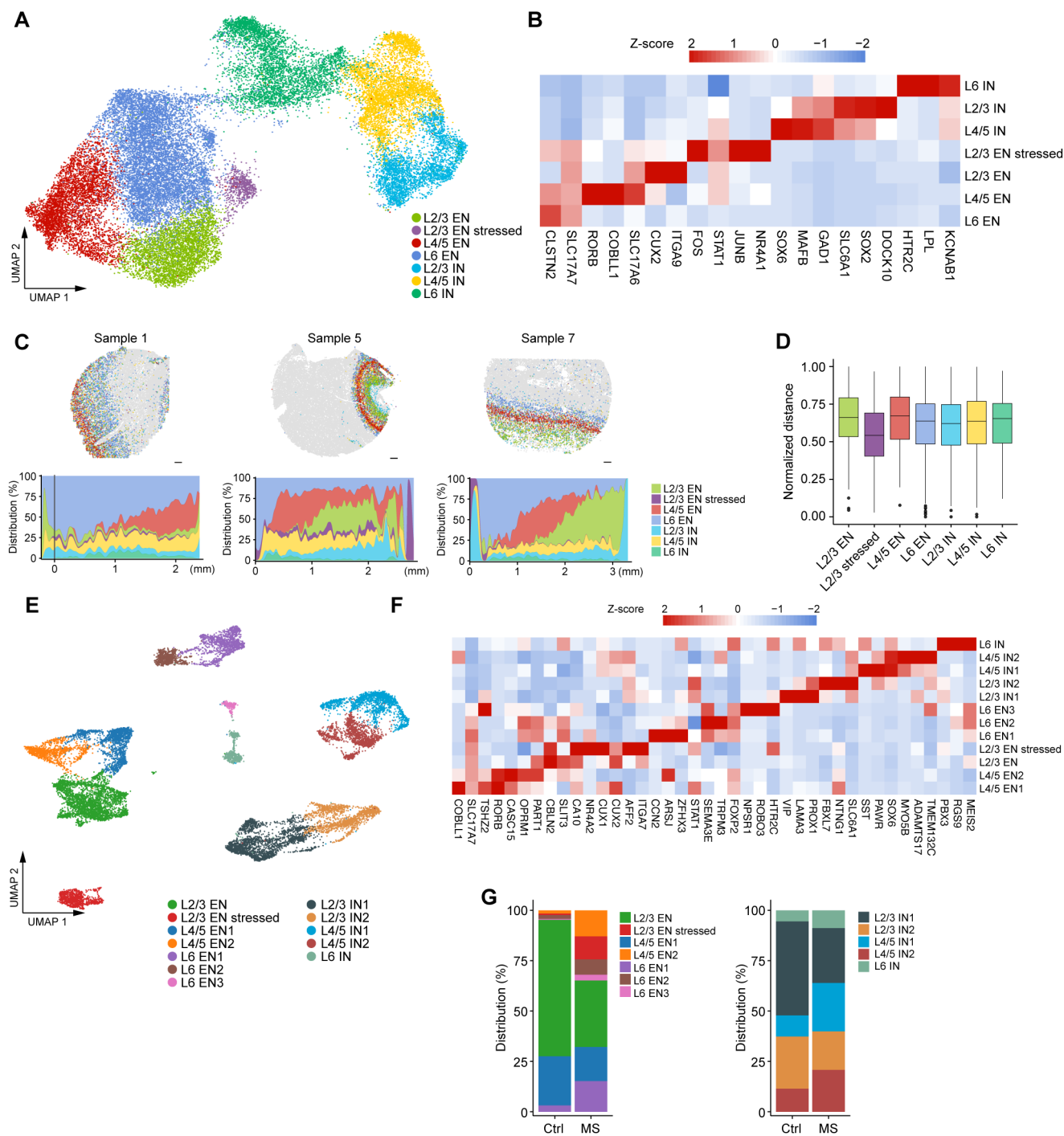
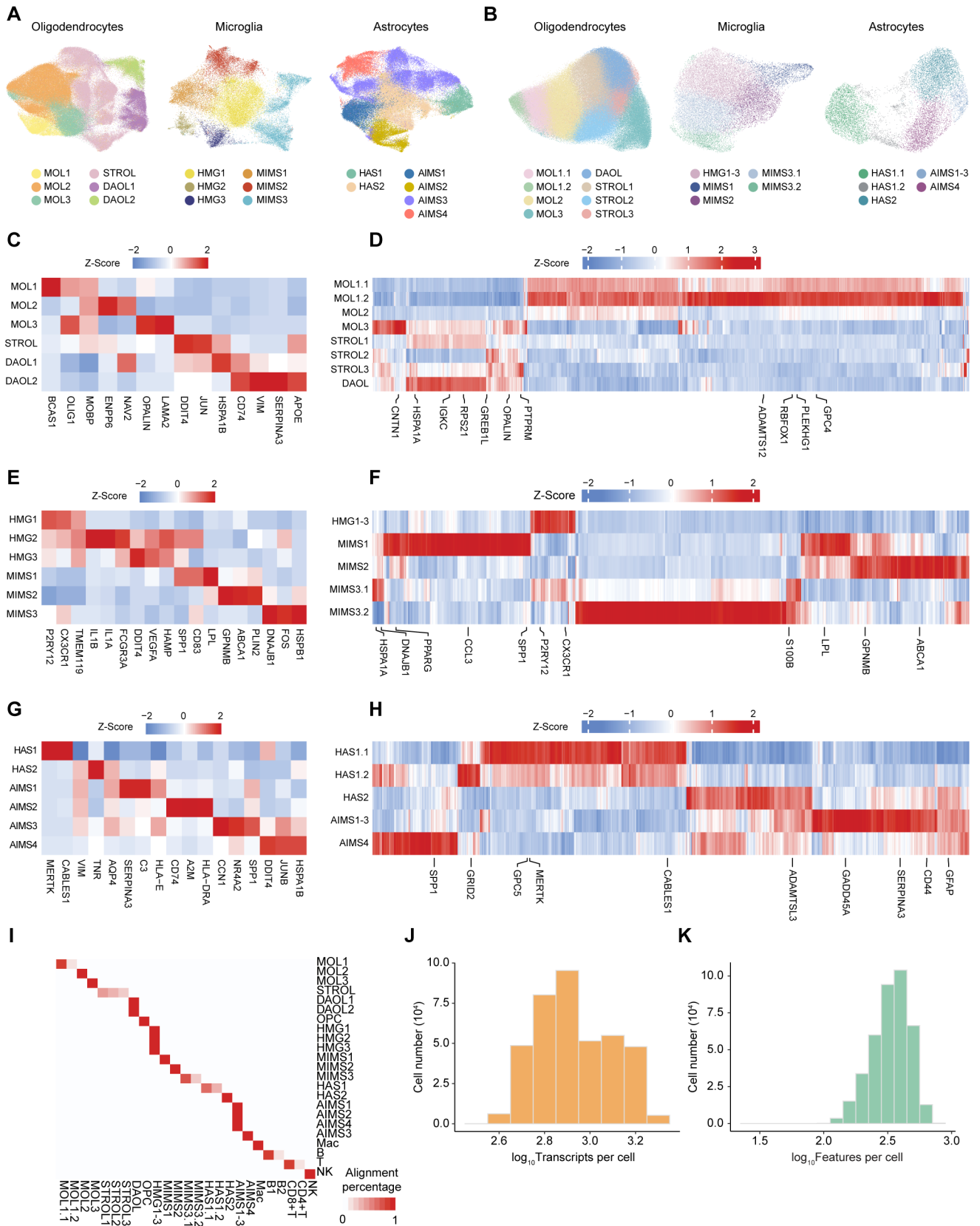
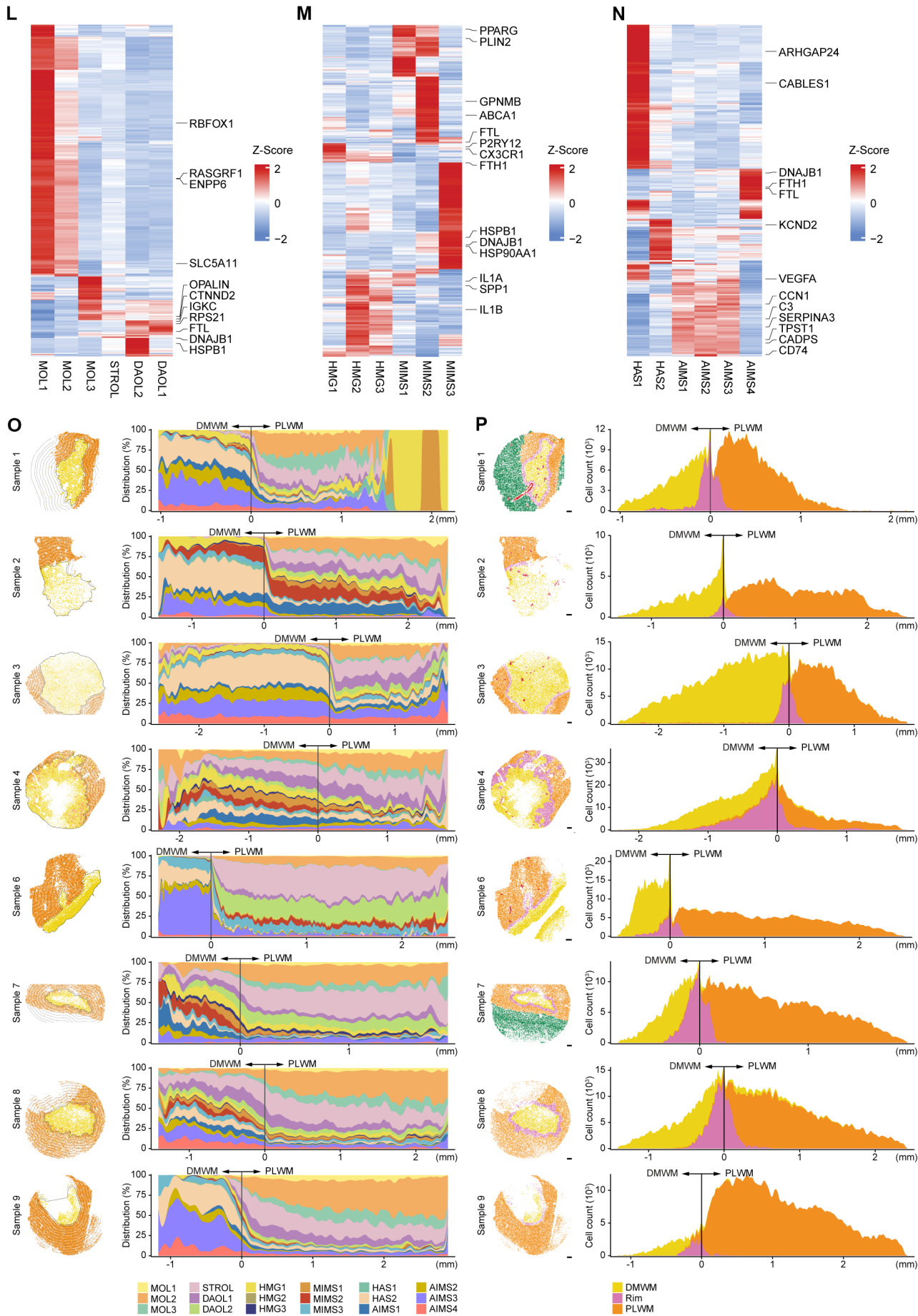


Figure S2. Spatially resolved single-cell transcriptomic characterization reveals neuronal vulnerability in chronic active MS, Related to Figure 1

(A) UMAP projections for sub-clusters of excitatory and inhibitory neurons as identified by MERFISH.
 (B) Heatmap of scaled average expression for selected marker genes of neuronal sub-clusters in the MERFISH dataset.
 (C) Top: spatial mapping of neurons identified by MERFISH and projected onto 3 sections from different MS patients containing grey matter domains. Scale bars, 400 μ m. Bottom: density plots illustrating the distribution of neurons along the SPATA2 spatial gradient, according to the annotation of the GM.
 (D) Box plot showing the normalized distance of different neuronal sub-clusters from the lesion.
 (E) UMAP projections for sub-clusters of excitatory and inhibitory neurons as identified by snRNA-seq.
 (F) Heatmap of scaled average expression for selected marker genes of neuronal sub-clusters in the snRNA-seq dataset.
 (G) Bar plot depicting the neuronal sub-cluster distribution between control and MS samples based on snRNA-seq.
 The box and whisker plot elements in the figure represent the following: center line, mean; box limits, upper and lower quartiles; whiskers, minimum to maximum values.





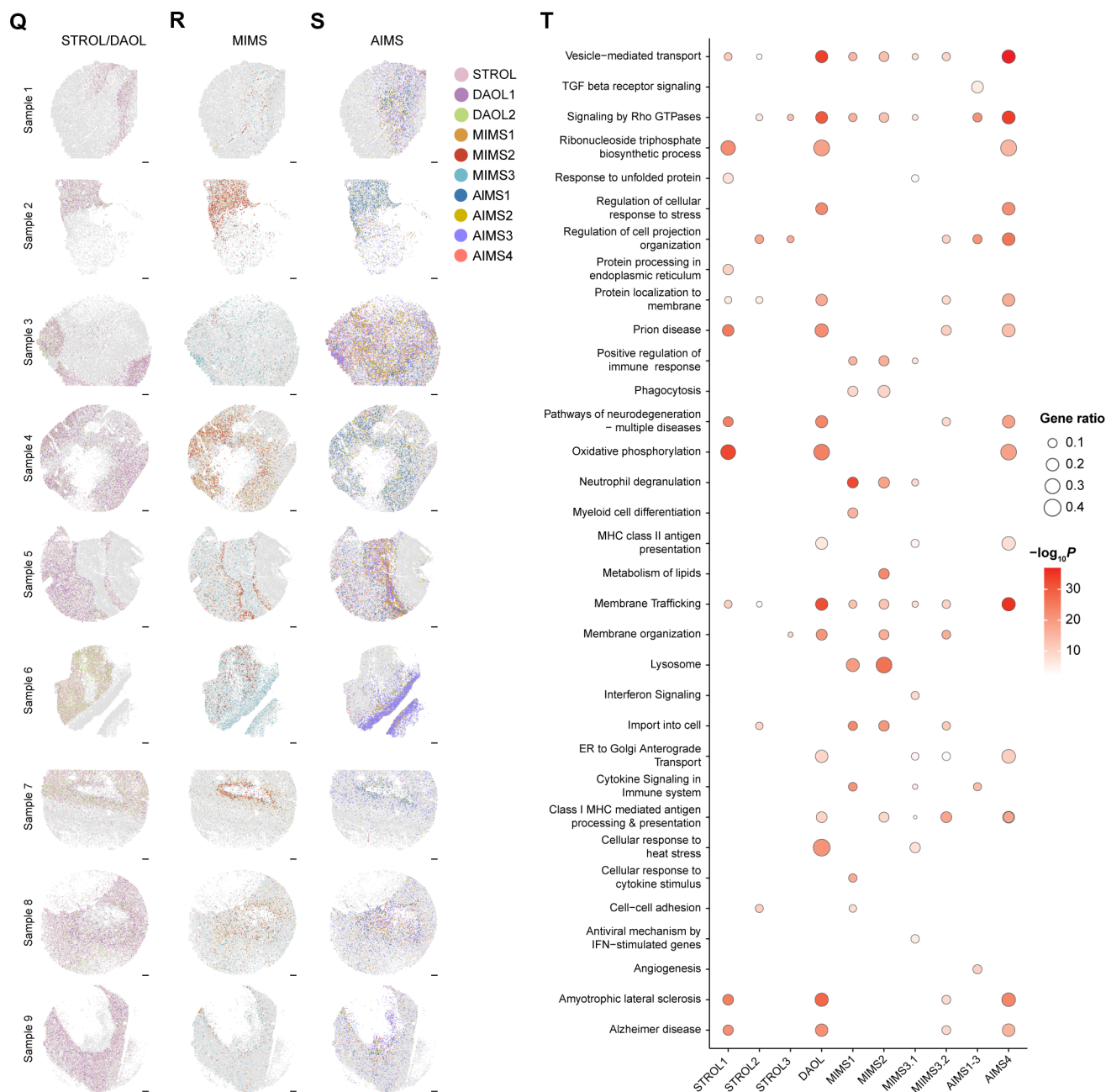


Figure S3. Spatially resolved single-cell transcriptomic characterization reveals glial cell states that define lesion domains in chronic active MS, Related to Figure 2

(A) UMAP projections for sub-clusters of oligodendrocytes (left, 177,015 cells), microglia (middle, 37,792 cells), and astrocytes (right, 78,755 cells) as identified by MERFISH.

(B) UMAP projections for sub-clusters of oligodendrocytes (left, 220,072 nuclei), microglia (middle, 23,376 nuclei), and astrocytes (right, 12,922 nuclei) as identified by snRNA-seq.

(C and E and G) Heatmaps showing the scaled average expression for selected marker genes of sub-clusters of oligodendrocytes (panel C), microglia (panel E), and astrocytes (panel G) in the MERFISH dataset.

(D and F and H) Heatmaps showing the scaled average expression for selected marker genes of sub-clusters of oligodendrocytes (panel D), microglia (panel F), and astrocytes (panel H) in the snRNA-seq dataset.

MOL, mature oligodendrocytes; STROL, stressed oligodendrocytes; DAOL, disease-associated oligodendrocytes; HMG, homeostatic microglia; MIMS, microglia inflamed in MS; HAS, homeostatic astrocytes; AIMS, astrocytes inflamed in MS.

(I) Heatmap showing the percentage of corresponding glial sub-clusters (oligodendrocytes, microglia, and astrocytes) and peripheral immune cell subsets from MERFISH and snRNA-seq datasets.

(J) Histogram showing the transcript counts and (K) feature counts of all cells in the imputed MERFISH dataset.

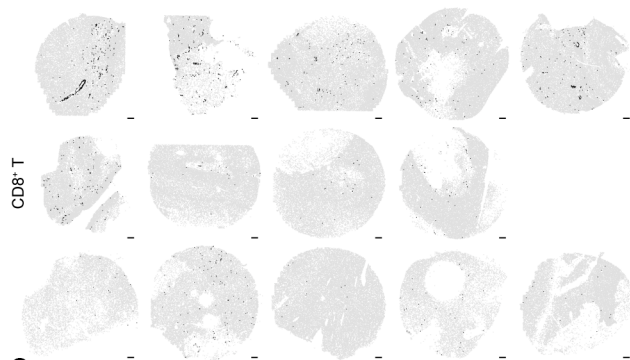
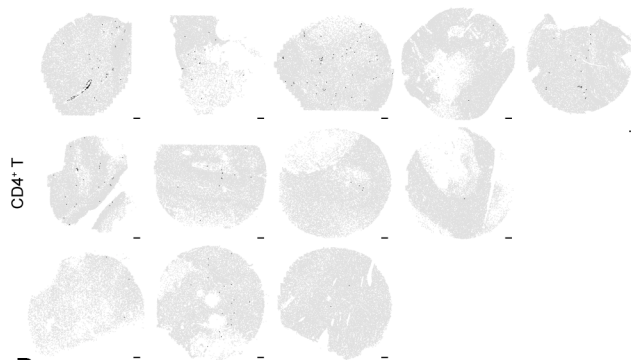
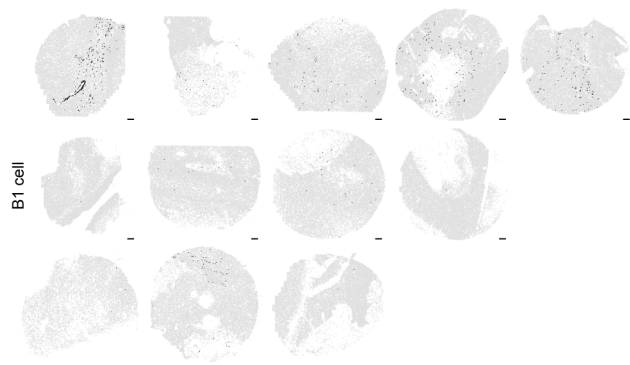
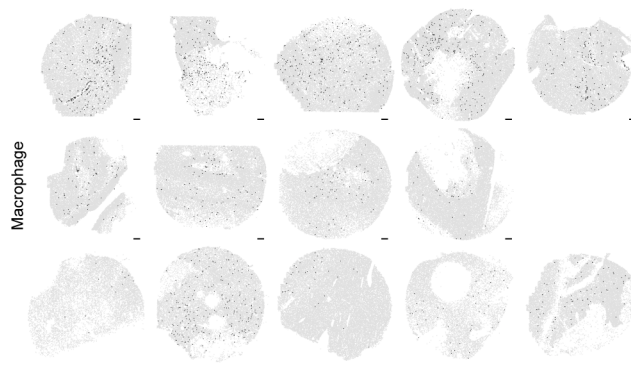
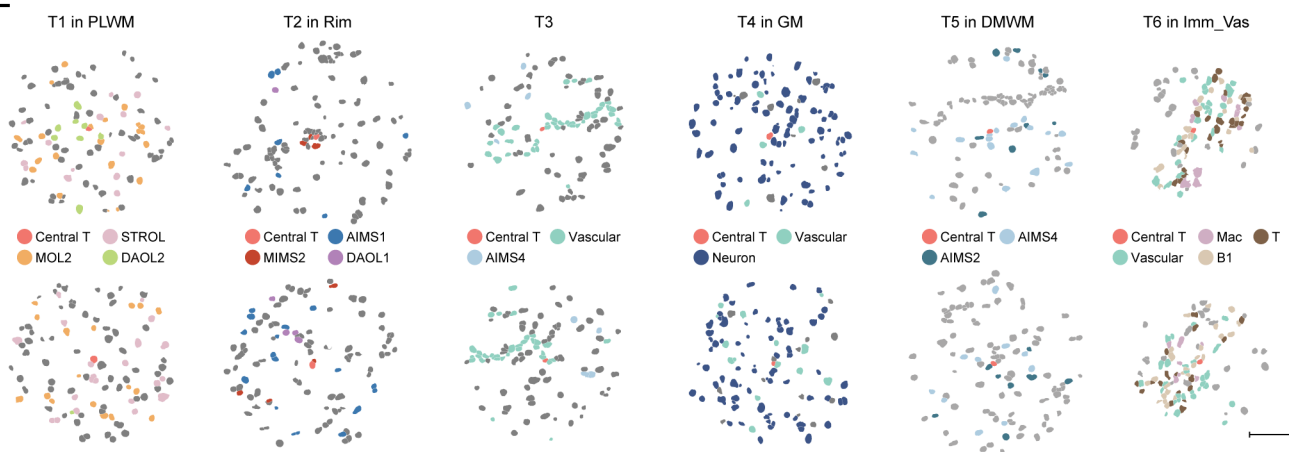
(L) Heatmaps of scaled average expression for selected marker genes of oligodendrocyte, (M) microglia, and (N) astrocyte sub-clusters in the imputed MERFISH dataset.

(O) Surface plots (left) and corresponding density plots (right) illustrating the distribution of various glial states along the SPATA2 spatial gradient, according to the annotations of the DMWM and PLWM in sections from 8 MS patients; inwards/outwards distances from the boundaries are indicated.

(P) Surface plots (left) and corresponding density plots of cell counts along the SPATA2 gradient (right), colored by the refined BANKSY domain segmentations including the lesion rims; inwards/outwards distances from the boundaries are indicated. Scale bars, 400 μ m.

(Q and R and S) Spatial mapping of reactive/disease-associated oligodendrocyte (panel Q), microglia (panel R), and astrocyte (panel S) sub-clusters projected onto the sections from 9 MS patients containing DMWM domains. Scale bars, 400 μ m.

(T) Dot plot showing selected terms from Metascape analysis of all significantly enriched marker genes for reactive/disease-associated oligodendrocyte, microglia, and astrocyte sub-clusters in the snRNA-seq dataset. Dot size represents the number of genes from the input gene list that hit the Metascape term, and colour intensity represents the negative log P value from the hypergeometric distribution test by Metascape.

A**B****C****D****E**

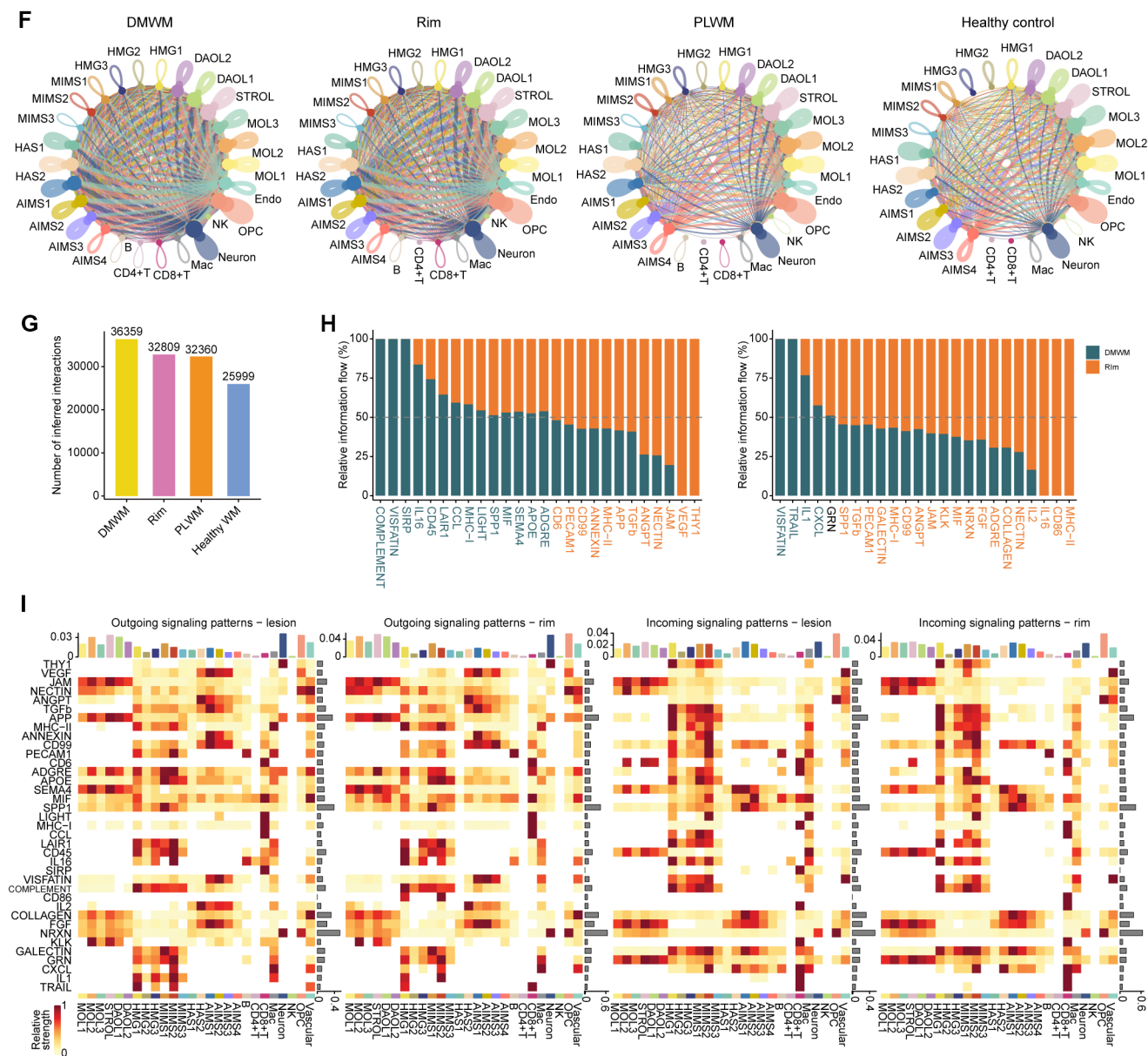
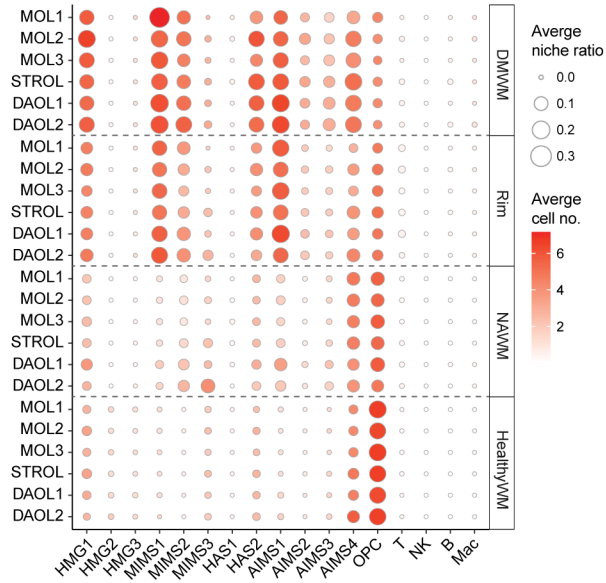


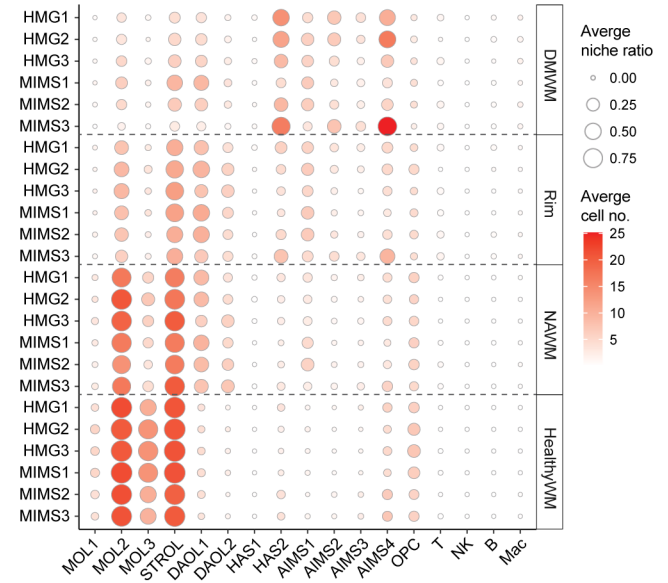
Figure S4. Spatially resolved single-cell transcriptomic characterization identifies peripheral immune cells and predicts cell-cell interactions in distinct lesion domains, Related to Figure 3

(A) Spatial mapping of CD8⁺ T cells (B) CD4⁺ T cells, (C) B cells, and (D) macrophages projected onto sections from 14 MS patients. Scale bars, 400 μ m. (E) High-resolution spatial mapping of different selected T cell niches in different lesion domains as segmented by BANKSY. Scale bar, 100 μ m. (F) Chord diagrams visualizing the strength of cell-cell signalling interactions between all annotated clusters in the DMWM, rim, PLWM, and healthy WM as segmented by BANKSY (imputed MERFISH dataset). The size of the node represents the number of cells, and the width of the edge represents the interaction strength between pairs of clusters. (G) Bar plot showing the number of cell-cell interactions between all annotated clusters in the DMWM, rim, PLWM, and control WM. (H) Bar plot showing the relative information flow of all signalling pathways from CD8⁺ T cells to all disease-associated microglia (MIMS1, MIMS2, and MIMS3; left) and from disease-associated microglia to CD8⁺ T cells (right) in DMWM (yellow) and rim (red). The height of each bar represents the normalized information flow. A paired Wilcoxon test was conducted to determine the significance of differences in information flow between the DMWM and rim. Significant differences are indicated by coloured labels of the respective pathway. (I) Heatmaps showing the relative signalling strength of cell groups in terms of outgoing and incoming signals. Row represents a selected signalling pathway, and column represents a cell group. The colour intensity in the heatmap corresponds to the strength of the signalling. The coloured bar plot (top) summarizes the total signalling strength of each cell group by aggregating all signalling pathways in the heatmap. The right bar plot shows the total signalling strength of each signalling pathway by aggregating all cell groups.

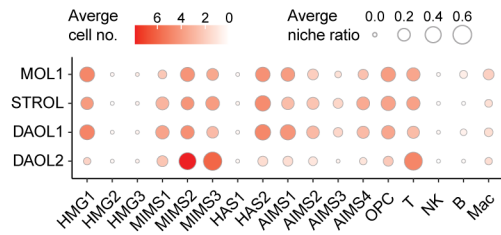
A



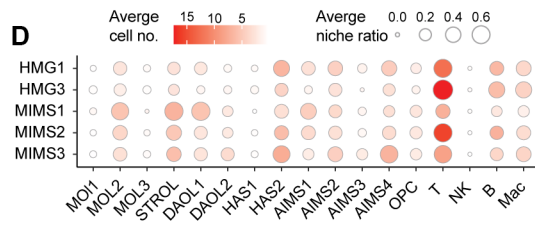
B



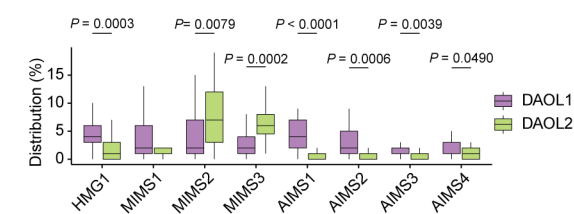
C



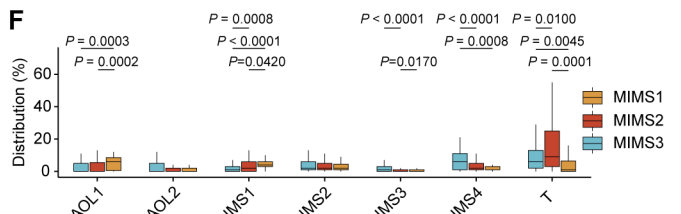
D



E



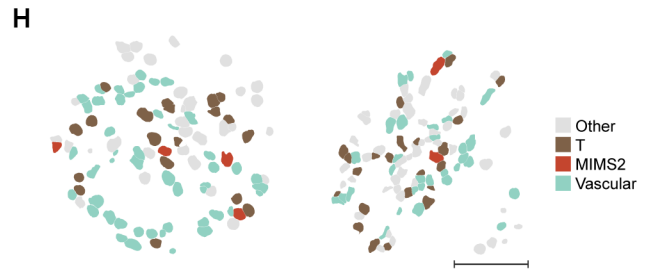
F



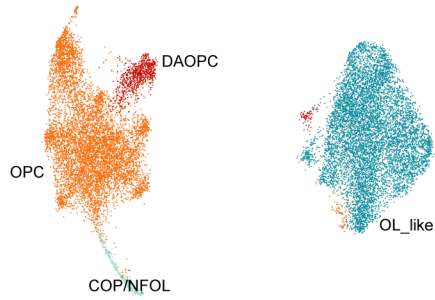
G



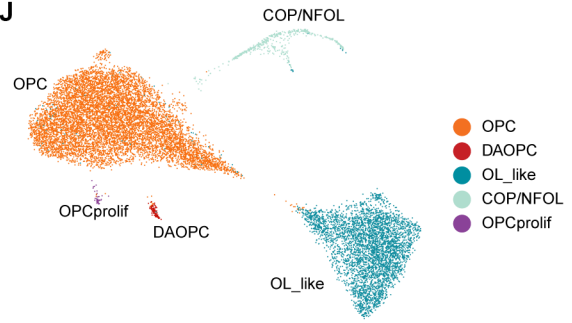
H



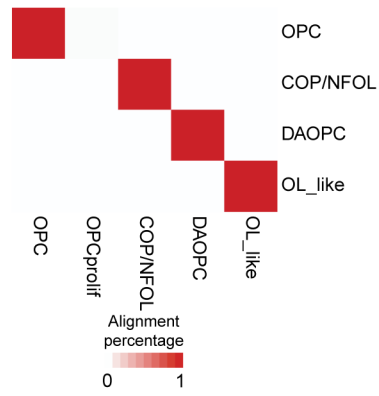
I



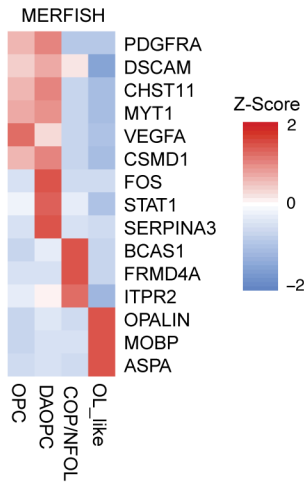
J



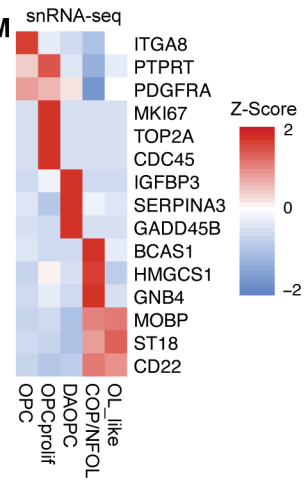
K



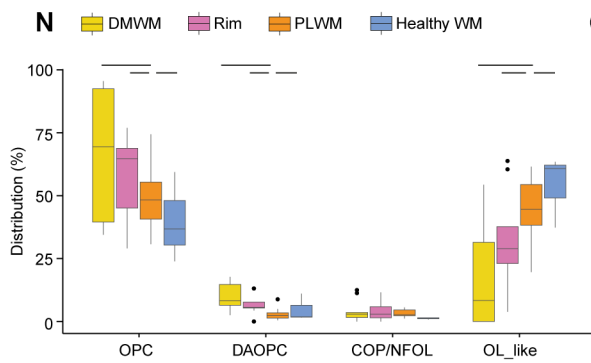
L



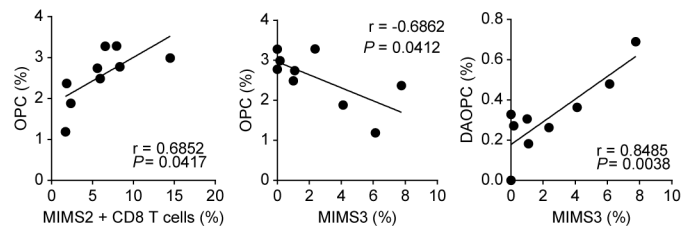
M



N



O



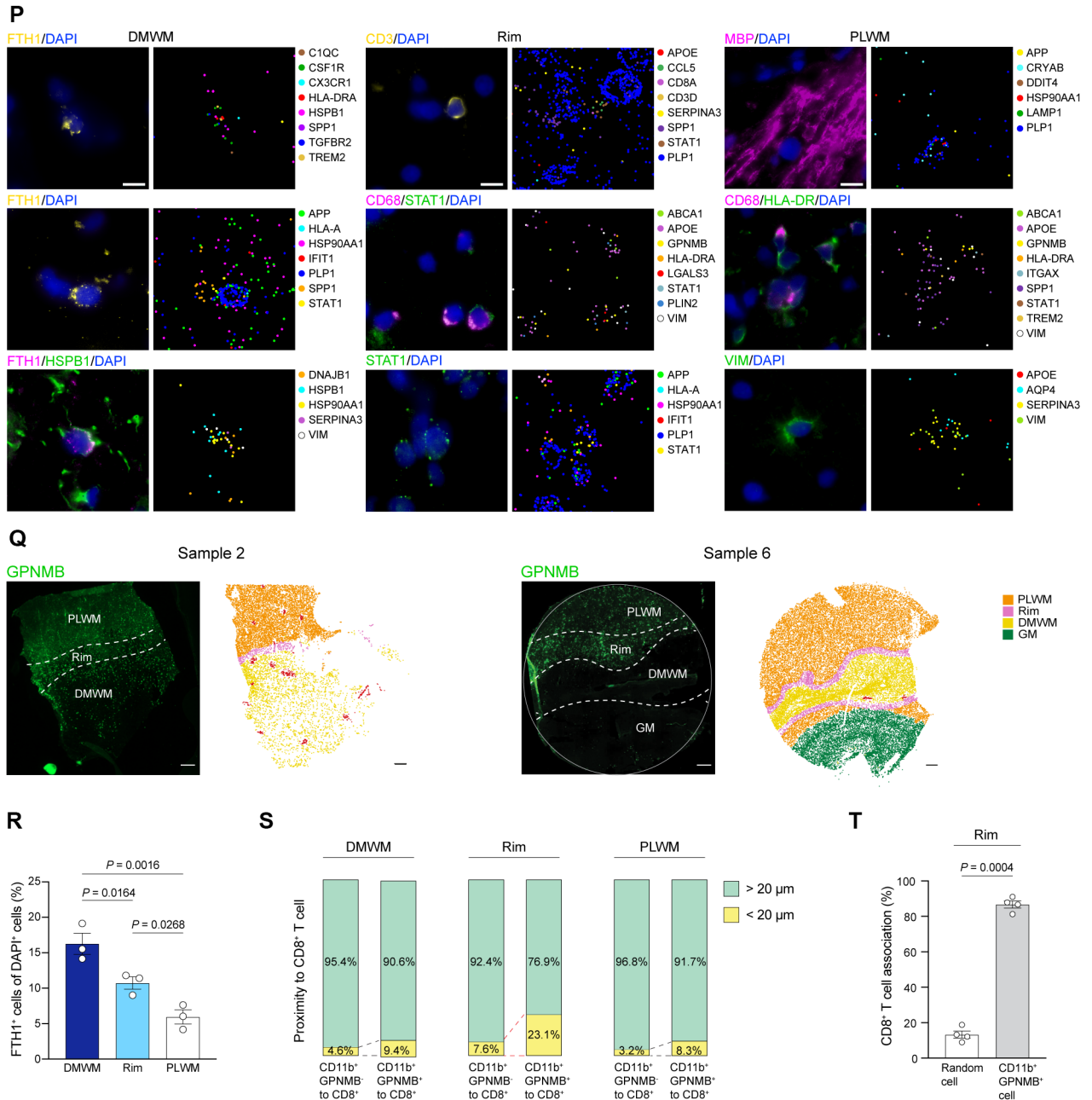


Figure S5. Distinct communities of oligodendrocytes, microglia and CD8⁺ T cells characterize different lesion domains in chronic active MS, Related to Figure 4

(A) Dot plot showing the composition of microglia sub-clusters, astrocyte sub-clusters, OPCs, and peripheral immune cell subsets for each oligodendrocyte sub-cluster niche in different white matter domains (DMWM, rim, PLWM, healthy WM). Dot color intensity represents the average cell number of sub-clusters in each oligodendrocyte niche and size represents the percentage of oligodendrocyte sub-clusters that contain at least 10 other clusters in their niche.

(B) Dot plot showing the composition of oligodendrocyte sub-clusters, astrocyte sub-clusters, OPCs, and peripheral immune subsets in each microglia sub-cluster niche in different white matter domains (DMWM, rim, PLWM, healthy WM). Dot color intensity represents the average cell number of sub-clusters in each microglia niche and size represents the percentage of microglia sub-clusters that contain at least 10 other clusters in their niche.

(C) Dot plot showing the composition of microglia sub-clusters, astrocyte sub-clusters, OPCs, and peripheral immune subsets in each oligodendrocyte sub-cluster niche in the Vas_Imm domain as segmented by BANKSY. Dot color intensity represents the average cell number of sub-clusters in each oligodendrocyte niche and size represents the percentage of oligodendrocyte sub-clusters that contain at least 10 other clusters in their niche.

(D) Dot plot showing the composition of oligodendrocyte sub-clusters, astrocyte sub-clusters, OPCs, and peripheral immune subsets in each microglia sub-cluster niche in the Vas_Imm domain as segmented by BANKSY. Dot color intensity represents the average cell number of sub-clusters in each microglia niche, and size represents the percentage of microglia sub-clusters that contain at least 10 other clusters in their niche.

(E) Box plot showing the distribution of selected microglia and astrocyte sub-clusters in the niche of disease-associated oligodendrocytes (DAOL1 and DAOL2) in the Vas_Imm domain as segmented by BANKSY.

(F) Box plot showing the distribution of selected oligodendrocyte and astrocyte sub-clusters, and T cells in the niche of disease-associated microglia (MIMS1, MIMS2, and MIMS3) in the Vas_Imm domain as segmented by BANKSY.

(G) Representative spatial mapping of selected cell types/sub-clusters in the niches of disease-associated oligodendrocytes or (H) microglia in the Vas_Imm domain as segmented by BANKSY. Scale bars, 100 μ m.

The box and whisker plot elements in the figure represent the following: center line, mean; box limits, upper and lower quartiles; whiskers, minimum to maximum values. Horizontal lines indicate statistically significant differences between groups as calculated with scCODA.

(H) UMAP projections for sub-clusters of OPCs (18,160 cells) as identified by MERFISH.

(I) UMAP projections for sub-clusters of OPCs (13,869 nuclei) as identified by snRNA-seq.

(J) Heatmap showing the alignment percentage of corresponding OPC sub-clusters from MERFISH (y axis) and snRNA-seq (x axis) datasets.

(K) Heatmap of scaled average expression for selected marker genes across all OPC sub-clusters in the MERFISH dataset. (E) Heatmap of scaled average expression for selected marker genes across all OPC sub-clusters in the snRNA-seq dataset.

(L) Box plot showing the distribution of different OPC sub-clusters (MERFISH dataset) for all samples in DMWM, rim, PLWM, and healthy WM.

(M) Correlation analysis between different MIMS/T cell and OPC sub-clusters at the lesion rim ($n = 9$ individuals with MS, two-tailed Pearson correlation calculations).

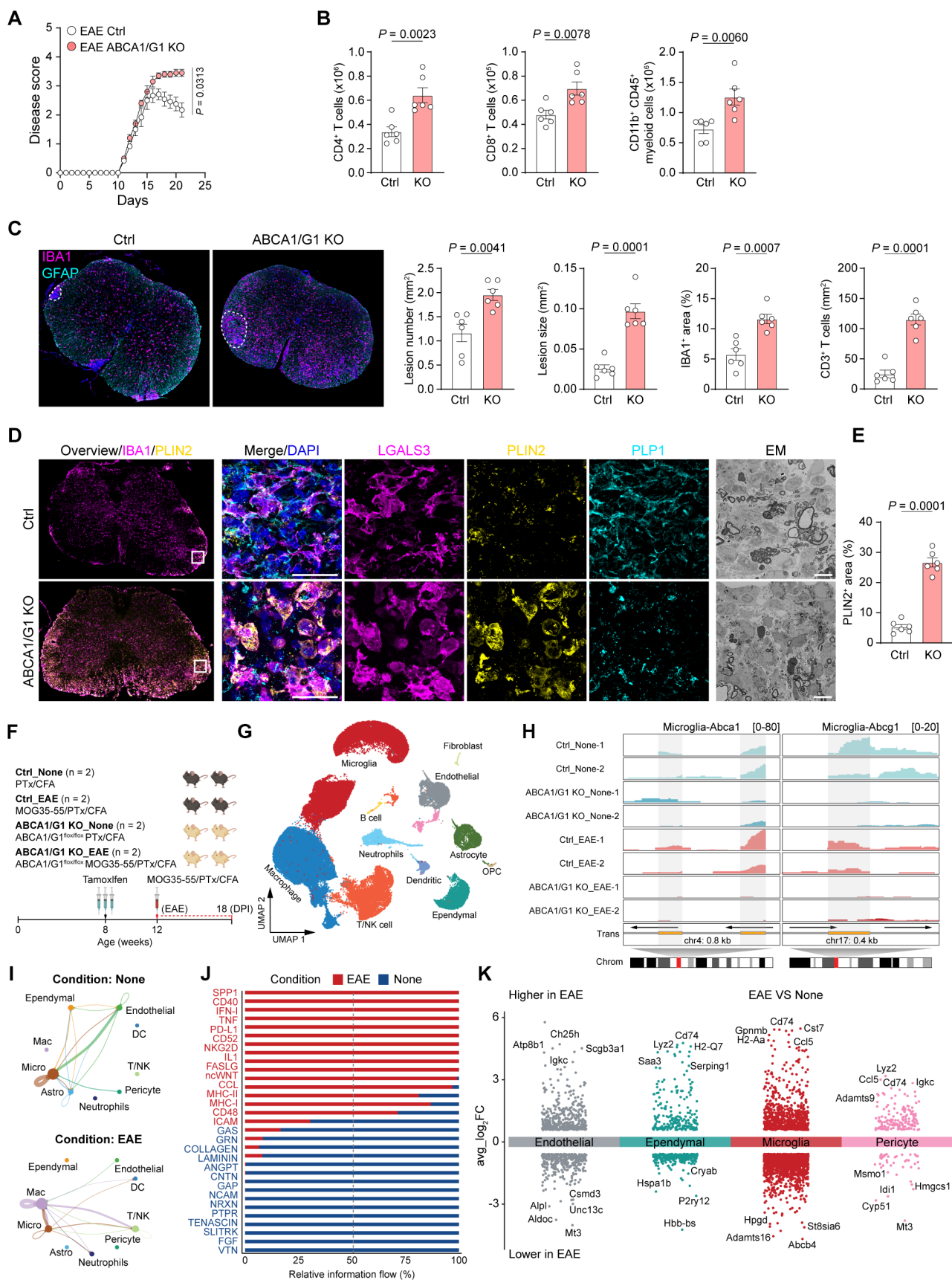
The box and whisker plot elements in the figure represent the following: center line, mean; box limits, upper and lower quartiles; whiskers, minimum to maximum values. Horizontal lines indicate statistically significant differences between groups as calculated with scCODA.

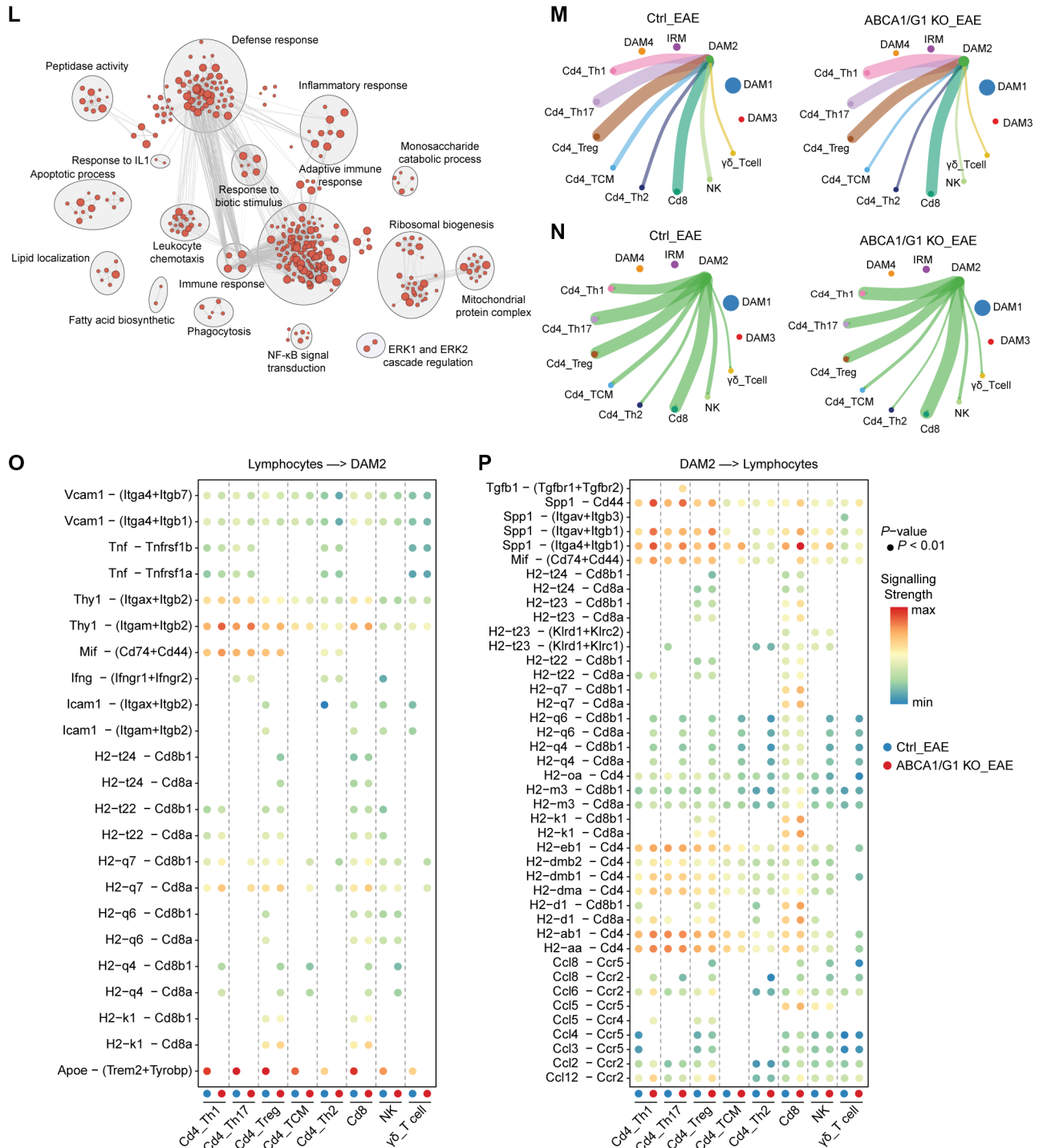
(N) Representative images of multiplexed protein co-detection in conjunction with MERFISH at distinct lesion domains. Protein detections indicating cell type or state in DMWM (left), rim (middle), and PLWM (right) are shown together with selected transcripts indicating cell type or state. Scale bar, 30 μm .

(O) Tile scans of immunofluorescence staining for GPNMB from two selected MS patients, highlighting three distinct domains (DMWM, rim, and PLWM) distinguishable by the GPNMB signal. Scale bars, 500 μm . Spatial projections of the different domains segmented by BANKSY using the MERFISH data of the two corresponding adjacent sections, illustrating how these regions were defined during quantification. Scale bars, 400 μm .

(P) Quantification of the percentage of FTH1⁺ cells among all cells within the DMWM, rim, and PLWM domains of MS patients ($n = 3$ individuals with MS, repeated measures ANOVA with Tukey's multiple comparison tests).

(Q) Bar plots showing the percentage of GPNMB⁺ and GPNMB⁻ CD11b⁺ cells in proximity to CD8⁺ T cells within the DMWM, rim, and PLWM domains of MS patients. (R) Quantification of the percentage of CD8⁺ T cells found in proximity to random cells compared with GPNMB⁺ CD11b⁺ cells ($n = 4$ individuals with MS, paired two-sided Student's *t*-test). Data are represented as the mean \pm SEM.





(F) Scheme depicting the strategy to induce microglia-specific ABCA1 and ABCG1 loss of function to ablate sterol efflux in MOG³⁵⁻⁵⁵ EAE and groups for scRNA-seq.

(G) UMAP projection of 88,812 cells from the scRNA-seq data of mouse spinal cord.

(H) Genome browser visualizations for the sequence read distribution of *Abca1* exon 45, 46 and *Abcg1* exon 3 in microglia under different conditions.

(I) Chord diagrams display the strength of cell-cell signaling interactions between all identified cell clusters in non-EAE (top) and EAE (bottom) groups. The size of the node represents the number of cells for a cell cluster, and the width of the edge represents the interaction strength between pairs of cell clusters.

(J) Bar plot showing the relative information flow of significant signaling pathways in non-EAE (blue) and EAE (red) groups. The height of each bar represents the normalized information flow. A paired Wilcoxon test was conducted to determine the significance of differences in information flow between the EAE and non-EAE group.

(K) Dot plot showing differentially expressed genes between EAE and non-EAE groups in selected major cell populations (endothelial, ependymal, microglia, and pericytes).

(L) Dot plot showing the enrichment map of significantly enriched GO terms and pathways from the different expressed genes between Control_EAE and Control_none groups. Nodes represent gene sets and edges represent degree of overlap between gene sets.

(M) Chord diagrams showing interaction strength of T cell subtypes to DAM2 microglia, and (N) interaction strength from DAM2 microglia to T cell subtypes in scRNA-seq data from EAE spinal cords using CellChat.

(O) Dot plots showing predicted significant signalling interactions from T cell subtypes to DAM2 microglia and (P) the predicted significant signalling interactions from DAM2 microglia to T cell subtypes.

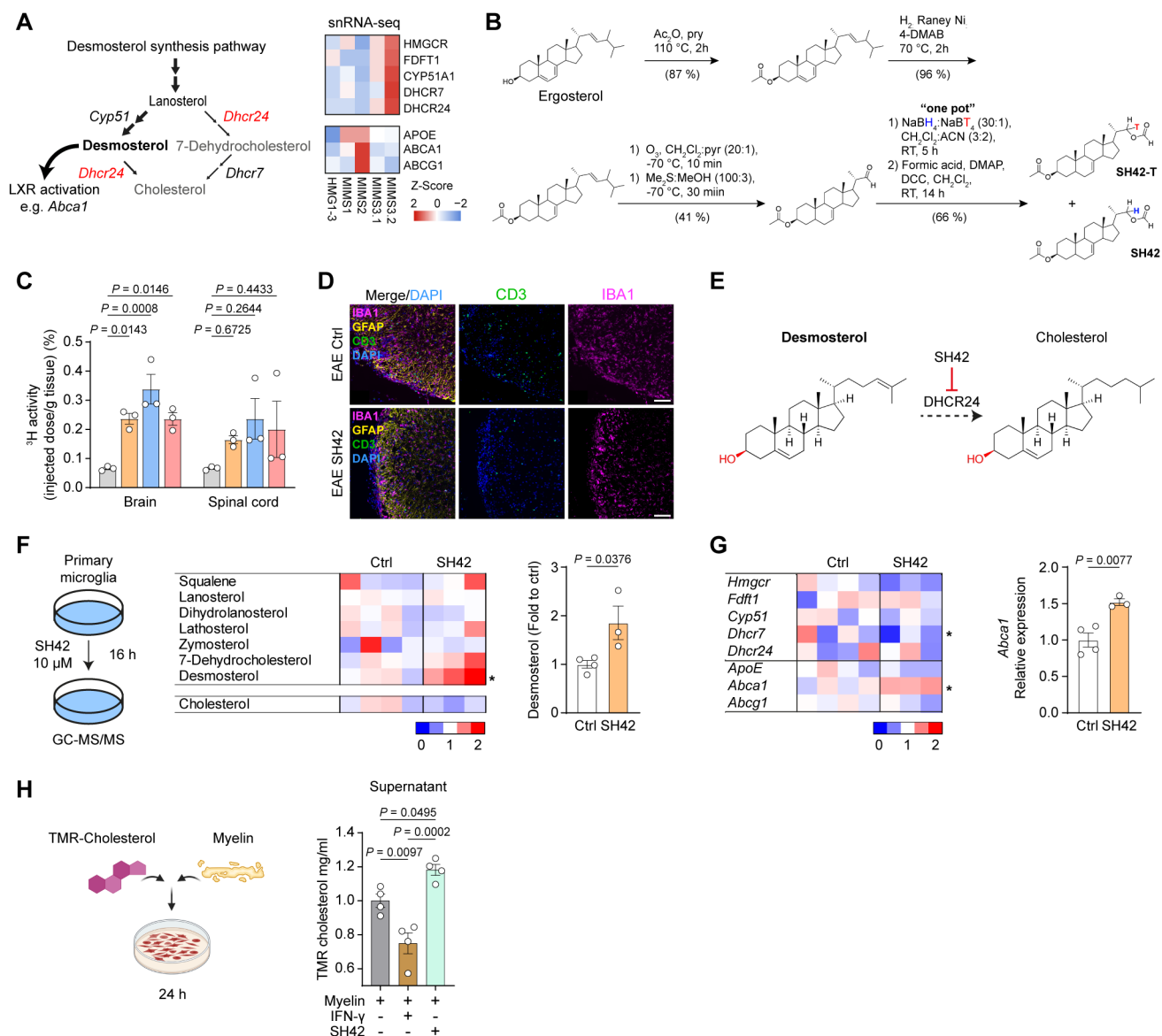


Figure S7. The DHCR24 inhibitor SH42 stimulates lipid efflux in the CNS, Related to Figure 7

(A) Scheme (left) depicting key enzymes and sterol synthesis intermediates of the desmosterol synthesis pathway regulating LXR activity in phagocytes. Active synthesis of the endogenous LXR ligand desmosterol (bold) is achieved by downregulation of the terminal sterol synthesis gene 24-dehydrocholesterol reductase (*Dhcr24*, red). Heatmap (right) showing expression of selected genes of the desmosterol synthesis pathway (*HMGCR*, *FDFT1*, *CYP51A1*, *DHCR7*, *DHCR24*) and LXR target genes (*APOE*, *ABCA1*, *ABCG1*) in human microglia from MS patients (snRNA-seq dataset).

(B) Schematic depicting synthesis of partially tritium-labelled SH42-T with modified protocol.

(C) Evaluation of substance delivery to the mouse brain and spinal cord by quantification of ³H activity at different time points (grey = 10 min, orange = 60 min, blue = 4 h, red = 8 h) after intraperitoneal administration. Data points represent values of individual mice (*n* = 3 mice per group, repeated measures ANOVA with Tukey's multiple comparison tests).

(D) Representative fluorescence images of CD3⁺ T cells in spinal cord EAE lesions of mice with or without SH42 treatment co-labelled with IBA1, GFAP, and DAPI.

(E) Schematic depicting the inhibition of DHCR24 by SH42 and affected sterols.

(F) GC-MS/MS analysis of primary microglia with or without 10 μM SH42 treatment. Heatmap (left) displaying the relative abundance of sterols normalized to controls. Bar graph (right) highlighting a selective increase of desmosterol after SH42 treatment. Data points represent individual cell culture experiments (*n* = 3-4 independent cultures, unpaired two-sided Student's *t*-test).

(G), RT-qPCR expression analysis of sterol synthesis genes (*Hmgcr*, *Fdft1*, *Cyp51*, *Dhcr7*, *Dhcr24*) and lipid efflux genes (*ApoE*, *Abca1*, *Abcg1*) of primary microglia as shown in panel e. Heatmap displaying relative expression values ($\Delta\Delta CT$ method) normalized to controls. Bar graph highlights increased *Abca1* expression after SH42 treatment. Data points represent individual cell culture experiments (*n* = 3-4 independent cultures, unpaired two-sided Student's *t*-test).

(H) Left: scheme depicting experimental design for the microglial cholesterol efflux assay. Right: Fluorometric measurement of TMR-cholesterol in supernatant of microglia 24h after treatment with myelin with or without IFN-γ and SH42 (*n* = 4 independent cultures per group, one-way ANOVA with Tukey's multiple comparison tests).

Data are represented as mean ± SEM.